Influence of electrode geometry on X-ray emission, plasma inductance, voltage, and current derivative signals obtained from a plasma focus device

Jalaj Jain [a,b,*], Jose Moreno [a,b,c], Biswajit Bora [a,b,c], Leopoldo Soto [a,b,c]

[a] *Comisión Chilena de Energía Nuclear, Casilla 188-D, Santiago, Chile*
[b] *Center for Research and Applications in Plasma Physics and Pulsed Power, P4, Chile*
[c] *Universidad Andres Bello, Departamento de Ciencias Físicas, República 220, Santiago, Chile*

A R T I C L E   I N F O

A B S T R A C T

Plasma focus devices have been investigated as a pulsed radiation source. Different studies have shown that the shape of the anode affects strongly the plasma dynamic and X-ray emission that takes place in plasma focus devices. In the present work, a hybrid-type plasma focus device (6 μF, 16 ± 1 kV), named PF-2kJ, is operated at various pressures of hydrogen gas with five cylindrical anodes of the same lengths but different in shapes, without cathode bars. The effect of cathode bars on various electric parameters is studied for the anode that has the maximum X-ray emission. The electrical signals of Rogowski coil (current derivative), voltage divider (voltage at the anode), and photomultiplier tubes (X-rays) were analyzed for all the anodes. Inductance and the voltage at the time of the pinch were derived from the measured voltage and current derivative signals. The X-ray dose measurements were performed using thermoluminescent dosimeters (TLD-100). The PF-2kJ performance is not the best while using the cathode bars. Our results show that by changing the anode shape just over the insulator sleeve the plasma focus devices can be switched between close energies stored in the capacitor bank.

Introduction

Plasma focus devices produce a pulsed plasma discharge of a duration of a hundred nanoseconds to few microseconds depending on the particular characteristics of the pulsed generator (capacitance, inductance, stored energy) [1,2]. The gas discharge takes place in a co-axial electrode geometry, in which the central electrode is kept partially covered by an insulator. During the first phase of plasma focus discharge, a plasma current sheet forms over the insulator surface. Under the action of the Lorentz force, the plasma current sheet runs over the effective length of the anode. At the open end of the anode, the plasma current sheet constricts by the self-generated magnetic field, compresses neutral gas ahead, and ionizes it. Such compression generates shock waves. At the axis of the anode, the shock waves reflect and slow down the compression. An equilibrium between compression and reflected shock waves produces a plasma column known as, pinch [1–3]. The model of compressing and reflected shock waves was given by S. Lee [4], which has to be verified experimentally. The above-mentioned plasma dynamics are observed in the electrical signals that will be shown and discussed in the result and discussion section of the present work. The duration of the pinch can be a few nanoseconds to tens of nanosecond depending on the pulse generator, with an electron temperature of the order of 0.5–1 keV and a density at the plasma focus axis of the order of 10^{19} cm^{-3}, independent of the energy of the device [2].

Various types of radiation; X-rays (low and high-energy) [5–9,3], neutrons (~MeV) [10–13,3], ions [14–17,3], relativistic electrons [18], UHF electromagnetic radiation [19–21] are emitted from the plasma focus devices. It is reported that at the time of compression and pinch formation electromagnetic fields and various types of instabilities generate the accelerated charged particles. Electrons move toward the anode and produce hard X-rays via bremsstrahlung on interacting with anode material. Ions move away from the anode. In the case of deuterium as working gas, the deuteron beams interact with background plasma/neutral deuterium gas and produce fast neutrons via beam-target nuclear fusion mechanism [22]. A fraction of thermonuclear neutrons is also reported [23–24]. It has been reported that the plasma electron density and temperature at the time of the pinch, the axial and radial speed of the plasma current sheet are similar in the plasma focus devices operated in a vast energy range; MJ to mJ [2]. Various schemes have been proposed to improve the performance of plasma focus devices concerning radiation emission [25,26]. Different anode geometries: oval-shaped anode, converging top anode, stepped anode have been

---

* Corresponding author.
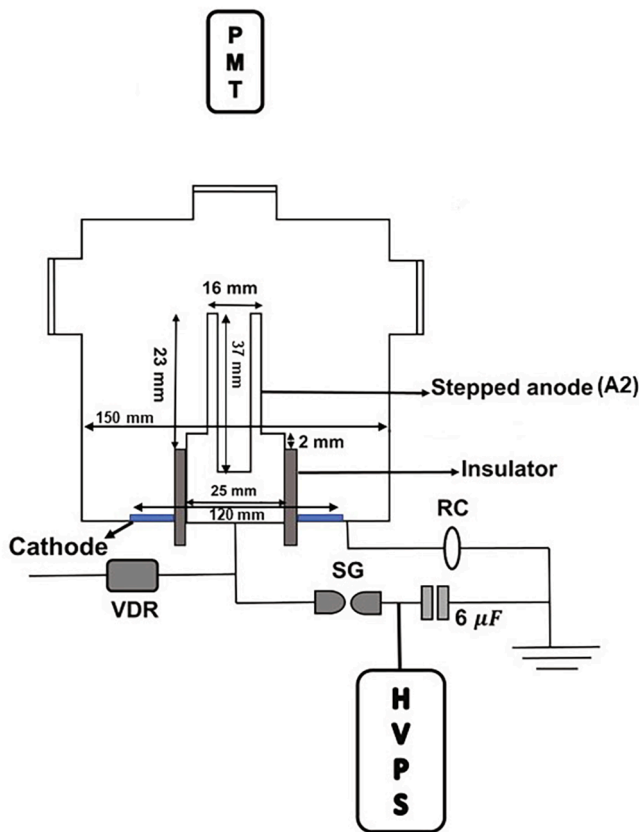*E-mail address:* jalaj.jain@cchen.cl (J. Jain).

Fig. 1. Schematic of the PF-2kJ with the mount of different diagnostics. RC: Rogowski coil, VDR: voltage divider, SG: spark-gap, HVPS: high-voltage power supply, PMT: photomultiplier tube.

voltage at the anode, and the X-rays in the axial direction were recorded. The plasma inductance and the voltage at the time of the pinch were derived from the voltage and current derivative signals using the methodology as described in references [33,34]. Various parameters such as rate of change of current at the time of pinch (dI/dt), voltage divider signals at the time of pinch (VDR), plasma voltage at the time of pinch (Vp), inductance at the time of pinch (Lp), the maximum current (Imax), the current at the time of the pinch (Ip), and the sum of the area under the curves of the X-rays pulses (AUC) were compared at each anode. At first, all five anodes were used without cathode bars. Later, twelve stainless steel cathode bars were introduced with the anode which yields the maximum X-ray emission. It is worth mentioning here that originally the size of the electrodes for the PF-2kJ was designed and built to be operated with a capacitor bank of 8 capacitors (1μF each), 17 kV (1.2kJ) [16]. Due to practical reasons, it was necessary to work with only 6 capacitors reducing the total capacitance to 6 μF to operate at 17 kV (867 J). Thus, the anodes were redesigned to fit with the generator without any other change, only the dimensions and shape of the anode over the insulator sleeve. On the one hand, the scope of the present work is to study how the plasma dynamics and behavior affect the radiation emission (X-ray) in a plasma focus discharge at different electrode geometries. For this purpose, it is studied different electrode configurations (different anode shapes, electrode assembly with and without cathode rods) at the same operational condition of the plasma focus device, PF-2kJ. From the electrical signals of the PF-2kJ discharge (voltage at the anode and current derivative) the current at the pinching time, plasma voltage evolution, and plasma contribution to the inductance are obtained and X-ray emission at different electrode configurations are compared. On the other hand, from the point of view of the applications of pulsed radiation emitted from plasma focus devices, it is desirable to accumulate large total doses in a short time, i. e. in few discharges. Such is the case of the applications in the study of pulsed radiation effects on biological samples, where the biological life material requires specific temporal and environmental conditions. Our laboratory has started research on this last topic [35]. The results presented here also could be of interest for other pulsed plasma and pulsed radiation research for example laser-produced plasma community.

Experimental setup

The main role of the cathode bars is to provide a return for the current in the conventional electrode configuration of the plasma focus device. In the case in which the radius of the cathode plate is greater than the radial expansion of the plasma current sheet during the first quarter of the period of the discharge, the plasma current sheet returns the current directly to the cathode plate, without cathode rods. Such is the case of the PF-2kJ used in these experiments and the cathode bars can be removed.

In Fig. 1, a schematic of the PF-2kJ with the mount of different diagnostics is shown. The anode (made of stainless steel) is a central
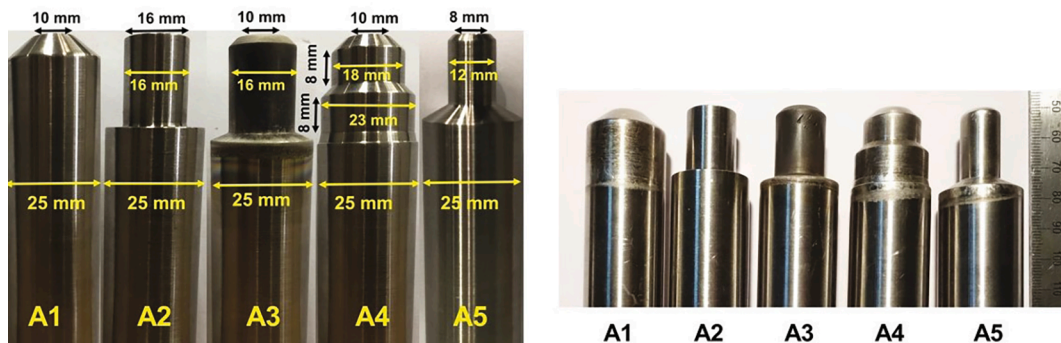
tested and it was reported that the converging top anode had a better performance [27]. The stepped anode was used to enhance the axial speed of the plasma current sheet, and the soft X-rays and neutron production were found axial-speed-dependent [28]. Apart from the change in the anode geometry, plasma focus devices have been operated with and without cathode bars [29]. In this work, the experiments are realized mainly without cathode bars. However, to verify the effect of cathode bars on X-ray emission, an electrode assembly including cathode bars is also used. Studies on the effects of insulator sleeve materials and lengths on plasma focus device performance are available in the literature [30–32]. In the present work, a 1.2kJ hybrid-type plasma focus, PF-2kJ (8 μF, 17 kV), is adopted to be work with 867 J (6 μF, 17 kV) by keeping the changes minimal in the PF-2kJ basic designs.

In the present study, five anodes of equal length and different shapes are used. The electrical signals; current derivative at the cathode, the

Fig. 2. Photographs of the anodes A1, A2, A3, A4, and A5.

Fig. 3. Electrode configuration with cathode bars. The anode A3 is used in this configuration.

electrode partially covered by an alumina insulator. The insulator length was ~37.4 mm. A capacitor bank of a total capacitance 6 μF was connected to one of the electrodes of the spark-gap (SG). The other electrode of the SG was connected to the anode of the PF-2kJ. A Rogowski coil (RC) was mounted around the cathode, a voltage divider (VDR) was mounted at the anode, and a photomultiplier tube (PMT) in combination with a scintillator (BC-408) was placed ~140 cm from the top of the anode in the axial direction.

Five cylindrical anodes that are used in the present work are shown in Fig. 2. All of the anodes had an equal length of ~80 mm but had different shapes. The anode A1 has a 25 mm diameter and converging top with a 10 mm inner diameter. The anode A2 has a diameter of 25 mm up to 2 mm above the insulator sleeve, then has a flat step with a diameter of 16 mm. The anode A3 has a diameter 25 mm up to the insulator sleeve, then has an angular step with a 16 mm diameter. The top of the A3 has a converging shape with a 10 mm inner diameter. The anode A4 has two steps. Until the insulator sleeve, the A4 has a 25 mm diameter, then with an angular step changes the diameter to 18 mm and a further step changes the diameter to 16 mm. At the top of the A4, the converging part has a 10 mm inner diameter. The anode A5 has a diameter 25 mm up to 3 mm above the insulator, then an angular step that changes the diameter to 12 mm. The open end of the A5 is converging with an inner diameter of 8 mm. The effective lengths of all the anodes are ~23 mm. In plasma focus devices electrons impinge upon the bottom of the anode and produce X-ray via bremsstrahlung. The bremsstrahlung X-ray emission increases with high atomic number target material for electrons. It is reported that the X-ray doses increase while inserting a lead piece inside the hollow anode [35], and the neutron yield increases by placing a conical tip in the centre of the anode end [36]. In the present work, all the anodes were kept hollow at the same depth ~37 mm so that a lead piece (working gas is hydrogen) can be inserted in the anode that yields the best performance.

At first, experiments were performed at various hydrogen gas pressures at each anode without cathode bars. Twenty discharges were shot at each anode-pressure combination. For example anode A1, pressure 5 mbar 20 discharges, 6 mbar 20 discharges, 7 mbar 20 discharges, 8 mbar 20 discharges, and so on; anode A2, pressure 5 mbar 20 discharges, 6 mbar 20 discharges, 7 mbar 20 discharges, and so on. All the analysis was performed with twenty discharges for each anode-pressure combination. Only the pressures at which pinch appeared are considered. The electrical signals such as; the voltage at the anode, the rate of change of current at the cathode, and the hard X-rays signals in the axial direction were captured at each pressure. Besides, dose measurements were performed in the axial direction using thermoluminescent dosimeters, TLD-100 at the anode which shows the maximum sum of the area under the curves of X-ray signals. The PF devices emit low (<10 keV) and high-energy X-rays (hundreds of keV), with a larger amount of low-energy
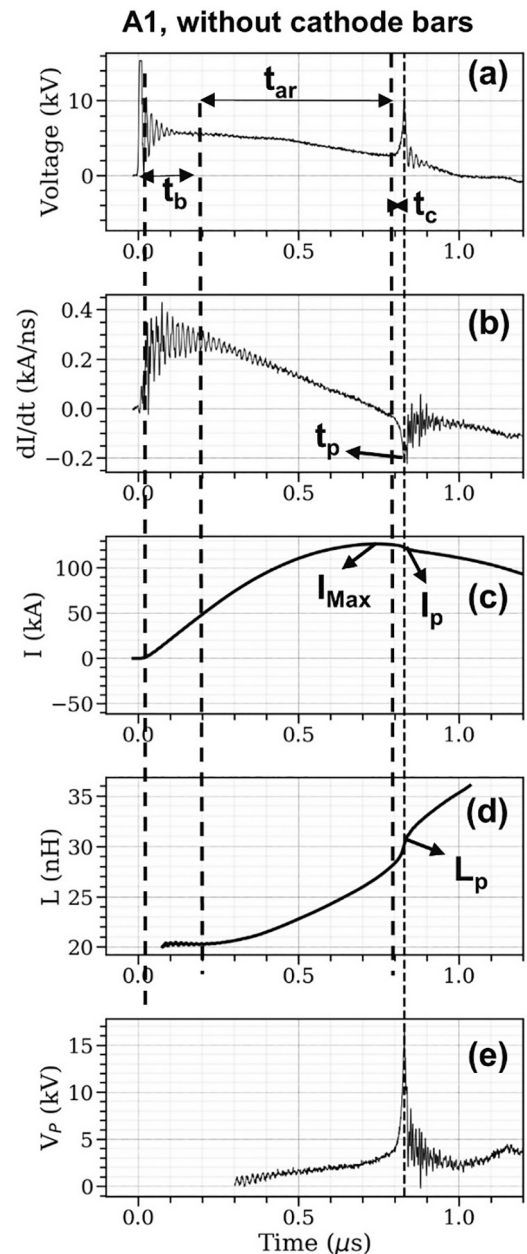

Fig. 4. Typical electrical signals. (a) Voltage at the anode, (b) current derivative at the cathode, (c) current (d) plasma inductance, (e) plasma voltage. The signals (a), (b) were recorded and (c), (e) were derived from the recorded signals.

X-rays [35]. Thus, for dose measurements, a vacuum window of ~0.8 mm high-density polyethylene plastic was prepared, over which the dosimeter array was kept at a distance ~7 cm from the open end of the anode (the plastic vacuum window will transmit X-rays of energies higher than 5 keV, thus in the obtained dose, X-rays in the energy range 5–10 keV contribute mainly, the negligible contribution of high-energy X-rays in doses is reported in the reference [35]). In a recent study, it is found that the Mather type plasma focus devices perform better while using the cathode bars [29]. To verify that we choose the anode that yields the maximum X-ray emission to work with cathode bars. It is worth to mention here that the PF-2kJ is a hybrid type (closer to Mather type) plasma focus device. Fig. 3 illustrates the electrode configuration with cathode bars.
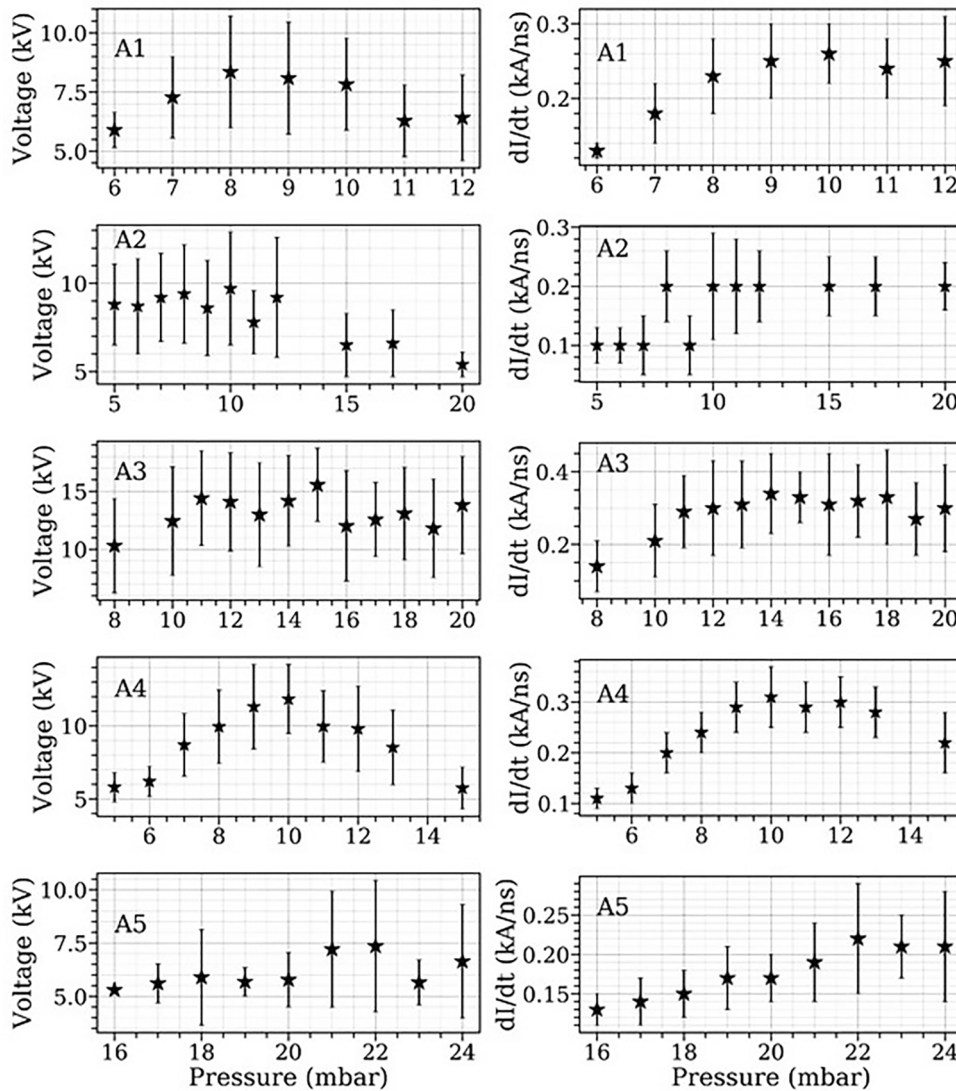
Fig. 5. Variation in the current derivative and voltage values (at the time of pinch) with pressures at different anodes.

Results and discussion

Electrical signals, plasma voltage, and plasma inductance.

The temporal evolution of the voltage at the anode (VDR) and the total current derivative dI/dt of the discharges were measured directly for all the pressures and different anodes studied. After, the current was obtained by integrating dI/dt signals numerically, and then the plasma inductance and the plasma voltage were derived from the signals VDR and dI/dt using the methodology as described in references [33,34]. It has been shown in references [3,34], the temporal evolution of the plasma inductance and plasma voltage gives information on the plasma behavior and plasma dynamics. In Fig. 4 typical signals of the (a) voltage at the anode (VDR) and the (b) dI/dt at the cathode at a pressure of 7 mbar of hydrogen gas are presented. The (c) current was obtained by integrating dI/dt signals numerically. The (d) plasma inductance and the (e) plasma voltage were derived from the signals (a) and (b). The description of Fig. 4 is as follows. The VDR signal falls rapidly at the beginning that indicates the gas breakdown. Later, the dI/dt reaches its maximum value that indicates closing the electrical circuit between the anode and cathode. Afterward, the resistive components will have a negligible influence on current flow, instead, the circuit will be inductive mainly as mentioned in reference [34]. During the time difference

t_b, (as shown in Fig. 4) the anode and cathode are connected electrically, and a plasma current sheet (PCS) forms over the insulator. The time t_b is considered during which the inductance varies slowly or stay constant in the inductance curve (Fig. 4(d)). Under the action of Lorentz force, the PCS runs over the effective length of the anode, which is known as the axial rundown phase, as shown by t_{ar} in Fig. 4. At the open end of the anode, a self-constricting Lorentz force acts on the PCS and the PCS compresses and ionizes the neutral gas ahead of it, which generates radial shock waves. On reaching the axis of the anode, the shock waves reflect that slows the compression and a plasma column forms known as the pinch. The compression and pinch times are shown by t_c and t_p in Fig. 4(a) and (b).

In the following, the variation in the above-mentioned electrical parameters with pressure is presented.

The voltage and current derivative at the time of the pinch

Fig. 5 shows the pressure dependence of the dI/dt and recorded voltage (VDR) at the time of the pinch (here the pressures at which the pinch appeared are presented). The standard deviations are large, and a conclusive peak is visible only for the anode A4, but the average values of the dI/dt and VDR signals at the time of the pinch are not the highest among all the anodes. For practical uses, pressure needs to be identified
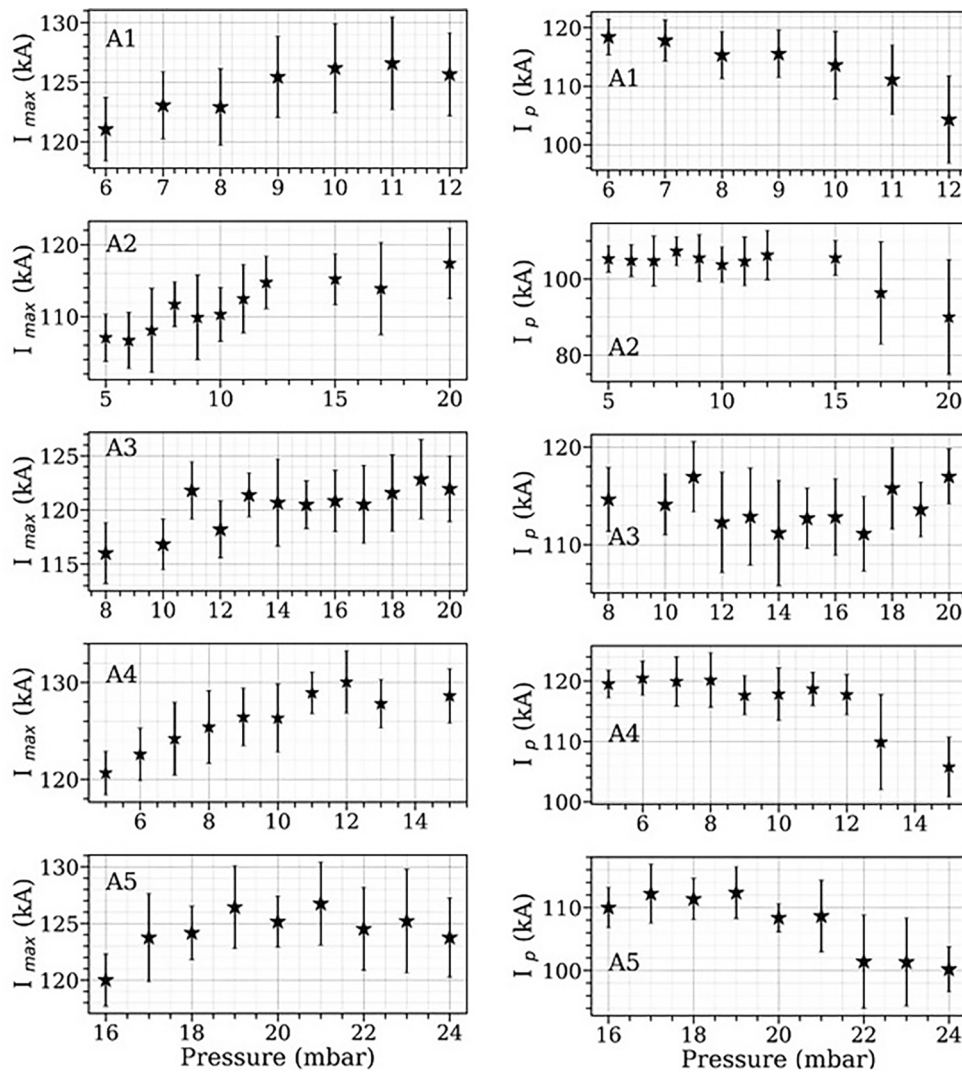
Fig. 6. Variation in the maximum current and the current at the time of the pinch with pressure.

at which the dI/dt and VDR signals show the highest amplitude of pinching action, which is taken care of by comparing the highest average values of the dI/dt and VDR signals among all the anodes. The VDR signals show the highest values (at the time of the pinch, t_p as shown in Fig. 4) at 8–9 mbar (anode A1), 10 mbar (anode A2), 15 mbar (anode A3), 10 mbar (anode A4), and 21–22 mbar (anode A5). The pressures at which the dI/dt signals acquire minimum values (at the time of the pinch, t_p, shown in Fig. 4) are 9–10 mbar (anode A1), 10 mbar (anode A2), 14–15 mbar (anode A3), 10 mbar (anode A4), and 22 mbar (anode A5). The dI/dt values at t_p are multiplied by (−1) for picture purposes.

Interestingly, the pressure range for the minimum values of the dI/dt and the maximum values of VDR signals at the time of the pinch, t_p, changes upon changing the anode. The pressure range to obtain the optimized pinch conditions relies on the effective length of the anode [1,2], which is the same for all the anodes in the present case. If the effective length is too large, the PCS will arrive at the open end of the anode at later times than the maximum current, therefore, the pinching action takes place at a later time then the maximum current. If the effective length is too short the PCS will arrive too early at the open end of the anode. The PCS arrival time at the open of the anode must coincide with the maximum current to have optimized pinch conditions. Such coincidence is required so that the maximum transfer of inductive energy to the pinch can take place. The A2 and A3 have similar shapes except, 1) the A2 has a diameter 25 mm until ~2 mm above the

insulator, in the case of the A3, the diameter of the anode was kept 25 mm until the insulator end. 2) The anode A2 has a flat top, but A3 has a converging top. At this moment it is not clear why the dI/dt and VDR signals at the pinching time, t_p, show peaks at different pressures in the case of the A2 and A3.

The anode A5 that has the smallest diameter at the position of the effective length, shows the highest value of the VDR and dI/dt signals at the time of the pinch, t_p, at 22 mbar of pressure. The current that flows in the circuit depends on the total capacitance, applied voltage, and inductance and does not depend on the anode shape. However, the current density will depend on the anode's surface area over which the current flows, which is the lowest in the case of the A5 and maximum in the case of the A1. Therefore, the current density at A1 will be lower than A5. Higher current density will have a larger Lorentz force in the case of the A5 that will cause higher axial speed at lower pressures. With such considerations we hypothesize that in the case of the A5, at the pressures lower than 15 mbar, the PCS axial speed will be larger so that at the time the PCS reaches the open end of the A5, it continues in the axial direction without compressing. That could be the reason that the optimized pinch conditions were not observed at the pressures lower than 15 mbar in the case of the A5. A future scope exists to prove our hypothesis using shadowgraphy images at lower pressures, which can record images of the moving PCS in the axial direction. The maximum value of the VDR signal at the time of the pinch, t_p, is obtained for the
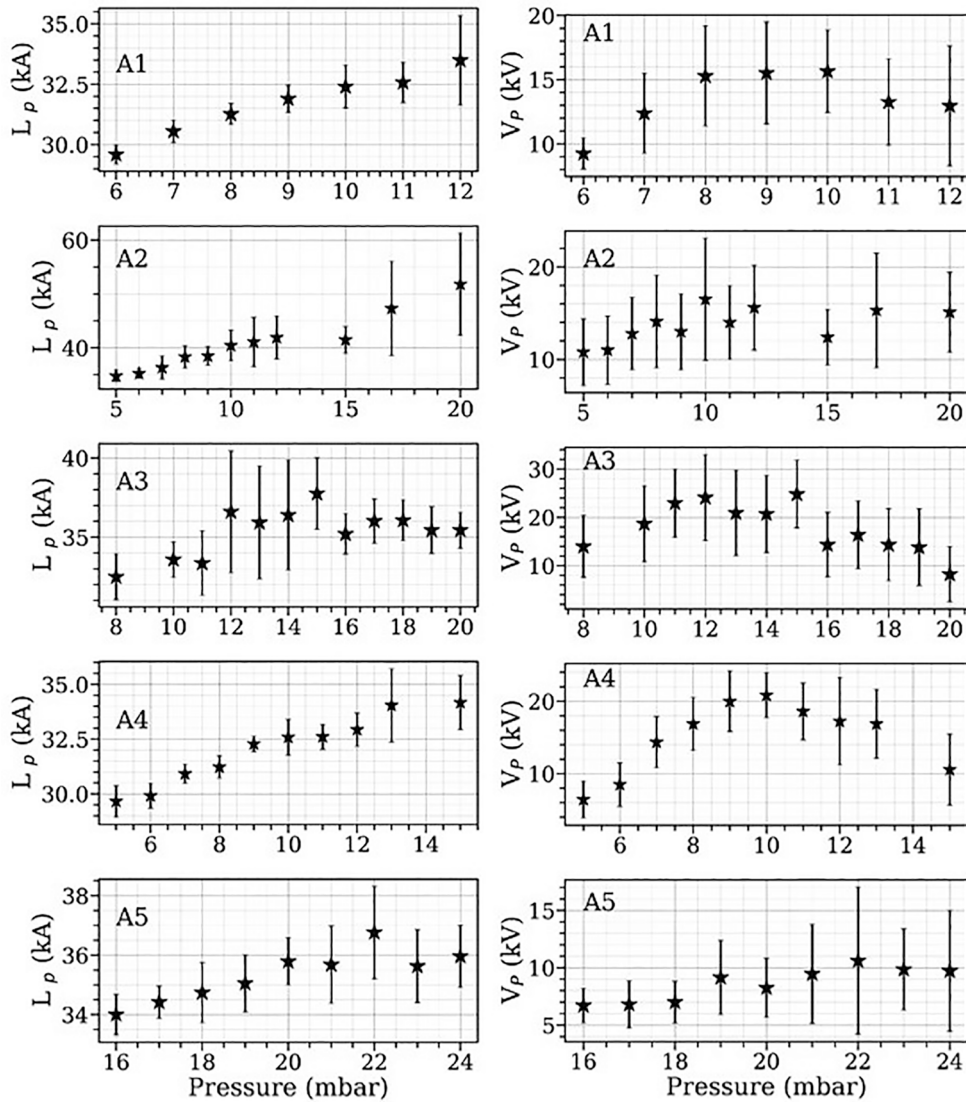
Fig. 7. Pressure dependence of the inductance at the time of the pinch and pinch voltage for the anodes A1, A2, A3, A4, and A5.

anode A3, whereas, the minimum dI/dt values at the pinching time, t_p, are similar for the anodes A2 (10 mbar) and A3 (14 mbar).

The maximum and pinch currents

Fig. 6 shows the pressure dependence of the maximum current (I_{Max}) and pinch current (I_P) for the anodes A1, A2, A3, A4, and A5. Generally speaking, the I_{Max} increases and I_P decreases with pressure, except for the anodes A3 and A5, with a small change in magnitude (10 kA difference). The variations in the I_{Max} and I_P are smaller in the case of the A3. At higher pressure, more neutrals will be available that will produce a larger number of ions and electrons, which will contribute to the maximum current. In the case of the anode A5, the I_{Max} rises until 19 mbar, and then fall after 21 mbar. At much larger pressures the electron mean free path will be lower and there is a possibility that the collisions take place before the electrons gain sufficient energy to ionize neutrals. Therefore, the I_{Max} will fall at such pressures.

The pinch inductance and pinch voltage

Fig. 7 shows the pressure dependence of the inductance at the time of the pinch (L_P) and the pinch voltage (V_P). The L_P increases with pressure for the anodes A1, A2, A4, and shows maximum values at 15 and 22
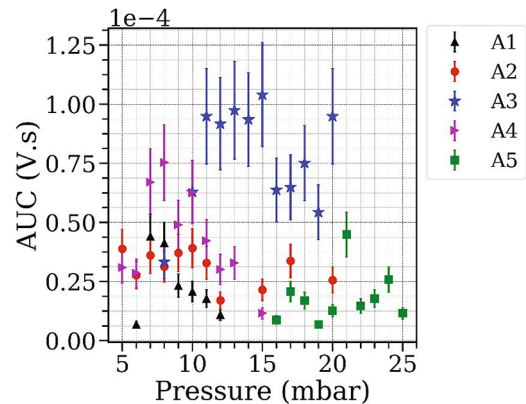

Fig. 8. Variation in the sum of the area under the curves of the X-ray pulses with pressure at different anode shapes. The anode A3 shows the maximum sum.

mbar for the anodes A3 and A5 respectively. The V_P shows maximum values at 8–10 mbar (A1), 10 mbar (A2), 15 mbar (A3), 10 mbar (A4), 22 mbar (A5). The decrement in the pinch current at the anodes A1, A2,
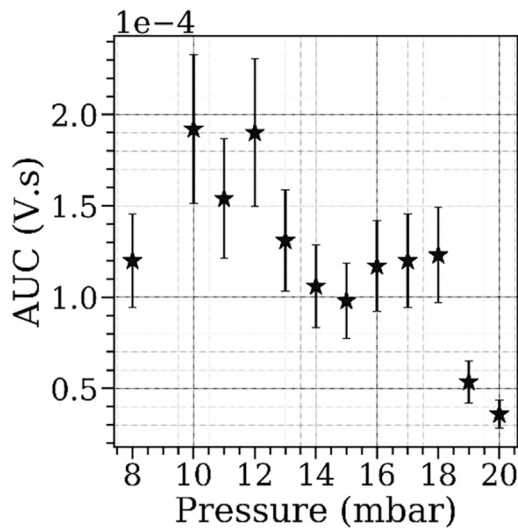
Fig. 9. Sum of the area under the curves of twenty X-rays pulses at various pressures (lead inserted inside the anode).
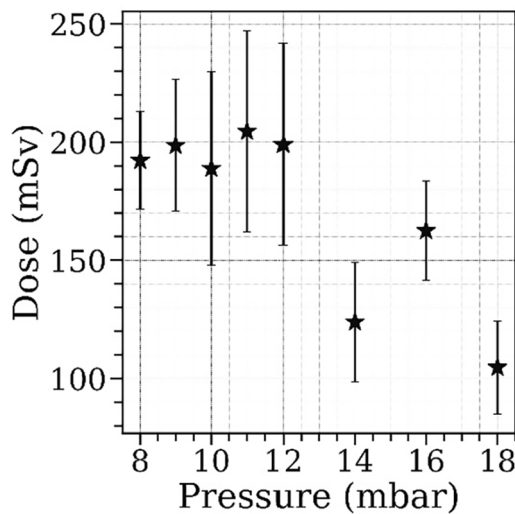

Fig. 10. Doses were obtained for twenty pulses of X-rays at various pressures.

A4, and A5 can be explained based on the fact that the inductance at that time increases with pressure for those anodes. The maximum value of V_P appears for the anode A3.

Sum of the area under the curves of the X-rays signals and dose measurements

In Fig. 8 the sum of the area under the curves (AUC) of photomultiplier tube signals (twenty shots) is presented. It is worth mentioning here that the sum of the AUC is considered so that it can be compared with the accumulated doses in the same number of X-ray pulses. The maximum sum appears at 15 mbar for the anode A3. With the above-mentioned information, dose measurements were performed using the anode A3. A lead piece was inserted inside the hollow anode to increase X-rays emission [35]. Twenty discharges (in the condition of lead inserted inside the anode A3) in the pressure range 8–20 mbar were shot and the AUC of photomultiplier tube signals were estimated at each pressure. Fig. 9 shows the variation in the sum of the AUC with pressure. The insertion of lead has changed the pressure range at which the sum of the AUC is maximum, which is 10–12 mbar. The possible reason could be the presence of lead impurities that will contribute to slowing down

the compression (additional material to be compressed) at larger pressures. Therefore, reduces the pressure to obtain an optimized pinching action.

Afterward, an array of six TLD-100 dosimeters was placed over a plastic vacuum window at ~7 cm from the top of the anode. Twenty pulses of X-rays were used to irradiate the dosimeters in the pressure range 8–18 mbar. Fig. 10 shows the obtained doses. The maximum doses were obtained in the pressure range 11–12 mbar, which coincides with the pressure range of the maximum sum of the AUC. Such dose characterization intended to use the PF-2kJ as a pulsed X-ray source to irradiate the different cancer cell lines *in vitro*.

It has been reported for a Mather type plasma focus device that it performs better in the co-axial electrode assembly [29]. In the following, the results of the co-axial electrode geometry (Fig. 3) using the anode A3, are presented. The anode A3 is chosen because it yielded the maximum X-ray emission.

PF-2kJ with co-axial electrode geometry

In Fig. 11, the electrical signals are shown in the cases of with and without the mount of the cathode bars (with the anode A3). The voltage, current derivative, and the estimated voltage at the time of the pinch show larger magnitudes in the case without the mount of the cathode bars. Besides, the inductance (d) during the radial compression presents a higher slope (higher derivative) that is a signature of a higher compression velocity for the configuration without cathode rods. In the following the pressure dependence of various electrical signals, measured and derived, is presented.

In Fig. 12, the pressure dependence of various electrical parameters that were obtained using co-axial electrode geometry (anode A3 was used) i.e. with the mount of 12 cathode bars (black filled circles), is shown and compared with the case without the mount of the cathode bars (blue stars). The voltage at the time of the pinch, dI/dt at the time of the pinch, estimated pinch voltage (V_p), and the sum of the AUC of X-ray signals have lower values in the case of co-axial electrode geometry. The dose measurements yielded ~60 mSv for 40 pulses of X-rays while using the co-axial electrodes. It is important to mention that the pinch and X-rays repetition was lower in the case of the co-axial electrode assembly. A total of 76 discharges were shot to get 40 X-rays pulses. In the case of without cathode bars, the X-rays repetition was about 100%. The PF-2kJ is a hybrid plasma focus device (closer to the Mather type). The plasma focus device that was used in reference [29] was a Mather type. Because of such geometrical differences, the PF-2kJ shows different behavior in comparison to the plasma focus device used in reference [29].

Conclusions

Different electrodes configuration (different anode shapes, electrode assemblies with and without cathode rods) at the same operational condition of the plasma focus device, PF-2kJ, were used and it was studied how the plasma dynamics and behavior affect the radiation emission (X-ray) under such electrode configurations. Electrical signals of the PF-2kJ discharge (voltage at the anode and total current derivative) were measured, and thus, the current at the pinching time, plasma voltage evolution, and plasma contribution to the inductance were obtained and X-ray emission at different electrode configurations were compared.

The following conclusions are drawn from the above-mentioned work.

– The pressure at which the sum of the area under the curves of the X-ray signals was maximum, does not coincide with the maximum magnitude of the current derivative and voltage signals at the time of the pinch for the anodes A1, A2, A4, and A5. Such conditions were met for the anode A3.
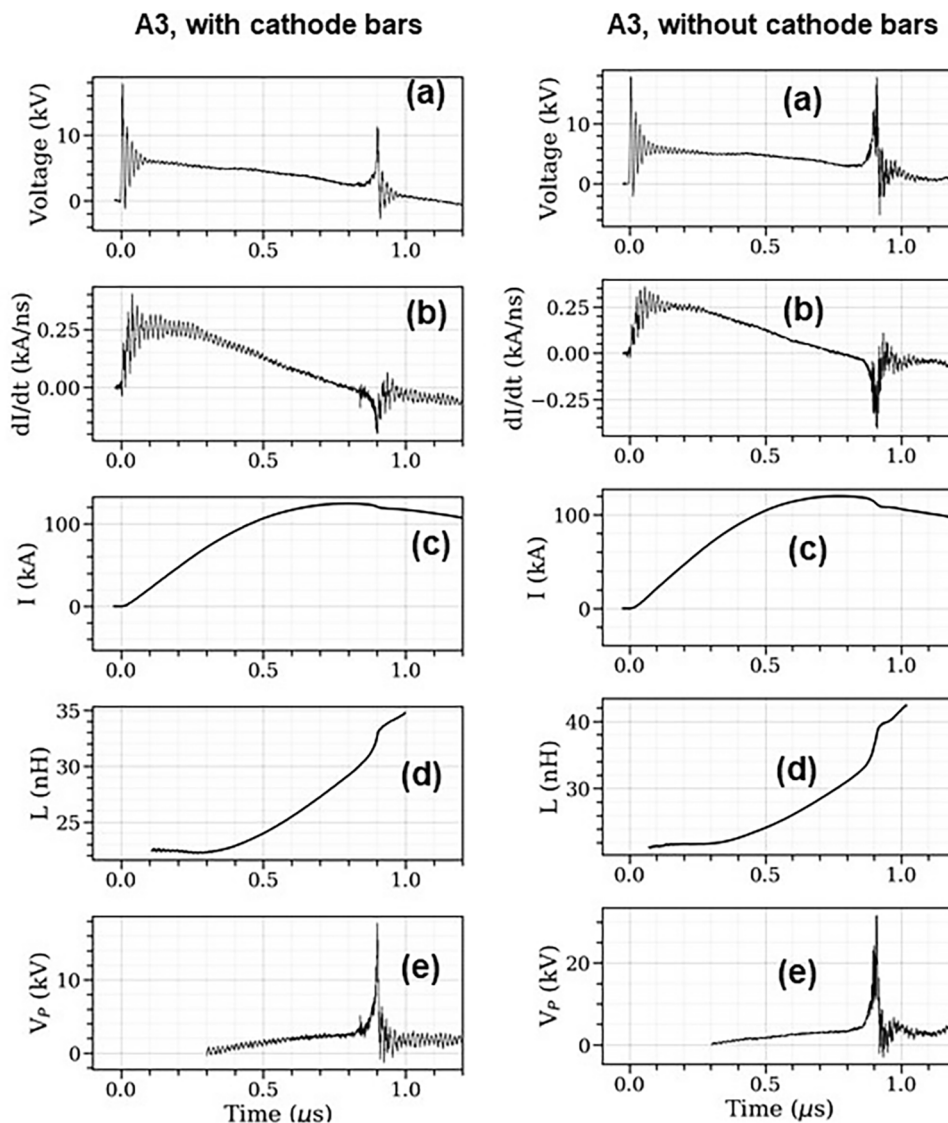
Fig. 11. Typical electrical signals were obtained in the case of with and without the mount of cathode bars in the PF-2 kJ at a pressure of 15 mbar of hydrogen gas. (a) voltage at the anode, (b) current derivative at cathode, (c) current (d) plasma inductance, (e) plasma voltage. The signals (a), (b) were recorded and (c)–(e) were derived from the recorded signals. The voltage and current derivative signals in the case of without cathode bars show larger magnitudes.

– The converging top anode (A3) yielded the maximum X-rays emission.
– The pressure range of the maximum dose coincides with the pressure range of the maximum sum of the area under the curves of the X-ray pulses.
– Observations of pinch and X-rays emission were found less frequently in the case of cathode bars are used in the present study.
– The voltage, current derivative, and the estimated voltage at the time of the pinch show a larger magnitude in the case without the mount of the cathode bars. In addition, the inductance during the radial compression presents a higher slope (higher derivative) that is a signature of a higher compression velocity for the configuration without cathode rods.
– Our results show that the plasma focus devices can be switched between close energies of the capacitor bank without changing the basic geometries such as-cathode plate and insulator sleeve, except changing the shape of the anode above the insulator sleeve. In the present work, the same geometrical and electrical parameters that were designed for 8 μF and 17 kV (1.2kJ) are used for 6 μF, 17 kV (867 J).

– The maximum X-ray emission conditions in plasma focus devices could be changed with the number of discharges. Therefore, a timely maintenance of the device is required to maintain such conditions.

CRediT authorship contribution statement

Jalaj Jain: Conceptualization, Data curation, Formal analysis, Investigation, Methodology, Funding acquisition, Writing - original draft. **Jose Moreno:** Data curation, Formal analysis, Funding acquisition, Supervision, Writing - review & editing. **Biswajit Bora:** Writing - review & editing. **Leopoldo Soto:** Formal analysis, Funding acquisition, Supervision, Writing - review & editing.

Declaration of Competing Interest

The authors declare that they have no known competing financial interests or personal relationships that could have appeared to influence the work reported in this paper.
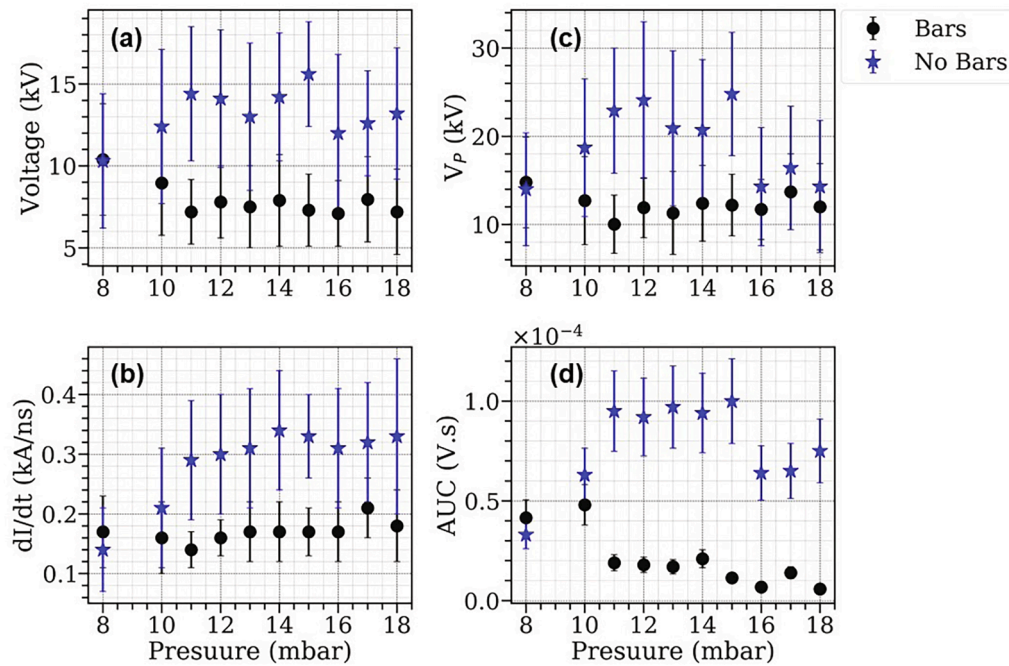
Fig. 12. Pressure dependence of the (a) recorded voltage at the time of the pinch, (b) dI/dt at the time of pinch, (c) estimated pinch voltage, (d) sum of the area under the curves of X-ray signals.

References

[1] Soto L. Plasma Phys Control Fusion 2005;47(5A):A361.
[2] Soto L, Pavez C, Tarifeño A, Moreno J, Veloso F. Plasma Sources Sci Technol 2010; 19:055017.
[3] Bernard A, Bruzzone H, Choi P, Chuaqui H, Gribkov V, Herrera J, et al. J Moscow Phys Soc 1998;8:93–170.
[4] Lee S, Serban A. IEEE Trans Plasma Sci 1996;24:1101.
[5] Jain J, Moreno J, Davis S, Bora B, Pavez C, Avaria G, et al. Results Phys 2020;16: 102915.
[6] Pavez C, Pedreros J, Zambra M, Veloso F, Moreno J, Tarifeño-Saldivia A, et al. Plasma Phys Control Fusion 2012;54:105018.
[7] Moreno J, Veloso F, Pavez C, Tarifeño-Saldivia A, Klir D, Soto L. Plasma Phys Control Fusion 2015;57:035008.
[8] Favre M, Silva P, Choi P, Chuaqui H, Dumitrescu-Zoita C, Wyndham ES. IEEE Trans Plasma Sci 1998;26:1154.
[9] Barbaglia M, Bruzzone H, Acuna H, Soto L, Clausse A. Plasma Phys Control Fusion 2009;51:045001.
[10] Soto L, Silva P, Moreno J, Zambra M, Kies W, Mayer RE, et al. J Phys D Appl Phys 2008;41:205215.
[11] Silva P, Moreno J, Soto L, Birstein L, Mayer R, Kies W. Appl Phys Lett 2003;83: 3269.
[12] Soto L, Pavez C, Moreno J, Altamirano L, Huerta L, Barbaglia M, et al. Phys Plasmas 2017;24:082703.

[13] Tarifeño-Saldivia A, Soto L. Phys Plasmas 2012;19:092512.
[14] Decker G, Wienecke R. Physica 1976;82C:155.
[15] Bernstein MJ, Meskan DA, Van Paseen HLL. Phys Fluids 1969;12:2193.
[16] Moo SP, Chakrabarty CK, Lee S. IEEE Trans Plasma Sci 1991;19(3):515.
[17] Jain J, Moreno J, Davis S, Bora B, Pavez C, Avaria G, et al. Phys Plasmas 2019;26: 103105.
[18] Jakubowski L, Sadowski M, Zebrowski J. Nucl Fusion 2001;41:755.
[19] Orellana L, Ardila-Rey J, Avaria G, Diaz MA, Pavez C, Schurch R, et al. IEEE Access 2019;7:133043–57.
[20] Avaria G, Ardila-Rey J, Davis S, Orellana L, Cevallos B, Pavez C, et al. IEEE Access 2019;7:74899–908.
[21] Orellana L, Avaria G, Ardila-Rey J, Davis S, Schurch R, Pavez C. IEEE Access 2020; 8:79273–86.
[22] Jäger U, Herold H. Nucl fusion 1987;27(3):407.
[23] Klir D, Kubes P, Paduch M, Pisarczyk T, Chodukowski T, Scholz M, et al. Plasma Phys Control Fusion 2011;54(1):015001.
[24] Klir D, Kubes P, Paduch M, Pisarczyk T, Chodukowski T, Scholz M, et al. Appl Phys Lett 2011;98(7):071501.
[25] Thein A, Kitagawa Y, Takahashi R, Yokoyama M. Jpn J Appl Phys 1977;16:1009.
[26] Kitaoka H, Sakurai A, Yamamoto T, Shimoda K, Hirano K. J Phys.Soc Jpn 1995;64: 4191–5.
[27] Talukdar N, Neog NK, Borthkur TK. Results Phys 2013;3:142–51.
[28] Serban A, Lee S. J Plasma Phys 1998;60:3–15.
[29] Piriaei D, Javadi S, Mahabadi TD, Yousefi HR, Salar Elahi A, Ghoranneviss M. Phys Plasmas 2017;24:043404.
[30] Hussain S, Shafiq M, Badar MA, Zakaullah M. Phys Plasmas 2010;17(9):092705.
[31] Momenei M, Khodabakhshei Z, Panahi N, Mohammadi MA. J Theor Appl Phys 2017;11:59–62.
[32] Zakaullah M, Baig TJ, Beg S, Murtaza G. Phys Lett A 1989;137:39–43.
[33] Veloso F, Pavez C, Moreno J, Galaz V, Zambra M, Soto L. J Fusion Energy 2012;31: 30.
[34] Bruzzone H, Acuña H, Barbaglia M, Clausse A. Plasma Phys Control Fusion 2006; 48:609.
[35] Jain J, Moreno J, Andaur R, Armisen R, Morales D, Marcelain K, et al. AIP Adv 2017;7:085121.
[36] Kubes P, Paduch M, Cikhardt J, Cikhardtova B, Klir D, Kravarik J, et al. Zaloga Phys Plasmas 2017;24:092707.